Two-dimensional electronic structure $E_i(k_i^{\parallel},k_i^{\perp})$ of GaAs(001) studied by angle-resolved photoemission

Y. Q. Cai, A. P. J. Stampfl,* J. D. Riley, R. C. G. Leckey, B. Usher,† and L. Ley‡
Physics Department, La Trobe University, Bundoora Victoria, 3083 Australia
(Received 21 October 1991; revised manuscript received 4 May 1992)

Angle-resolved photoemission techniques have been used to study the occupied band structure of the As-terminated GaAs(001)-1×1 surface grown by molecular-beam epitaxy. The measurements were taken along the [100] azimuth and covered the photon-energy range 10–70 eV. Structure plots involving linear-muffin-tin-orbital (LMTO) calculated valence bands and free-electron-like final states (FELFS's) were used to interpret the acquired data, which included normal-emission spectra at various photon energies and off-normal-emission spectra at selected photon energies. A structure plot of initial energy (E_i) versus polar-emission angle (θ) was employed to interpret the two-dimensional electronic structure $E_i(k_i^{\parallel},k_i^{\perp})$ observed from off-normal-emission spectra, where $k_i^{\parallel}$ and $k_i^{\perp}$ are, respectively, the parallel and perpendicular components of the wave vector of the valence electrons to the sample surface. It was found that the majority of strong transitions could be explained as direct transitions from LMTO valence bands to primary or secondary cones of FELFS's. The FELFS model was found to have mixed success over the entire photon-energy range investigated. We show, in particular, that the assignment of transitions can be misleading if only normal-emission spectra are considered.

I. INTRODUCTION

The energy band structure of valence electrons is one of the most important electronic properties of semiconductors. In studies of the valence-band structure semiconductors, angle-resolved photoemission remains one of the most powerful techniques.[1] The ultimate goal is to determine the energy dispersion $E_i(\mathbf{k}_i)$ of the bulk states and of the surface states associated with different surface structures. There are two aspects to this task. The first is to distinguish between the bulk- and surface-related features in the spectra, and the second is to determine simultaneously both the initial energy E_i and the associated wave vector $\mathbf{k}_i$ of the valence electrons. There have been a number of reports on studies of GaAs(001) surfaces using angle-resolved photoemission for various surface reconstructions.[2–7] Various methods have been applied in the previous studies to identify surface-sensitive features in the spectra, including absorption and/or deposition of foreign atoms on the surface to quench surface-state emission,[4,6] comparison of spectra from different surface reconstructions,[2,5,6] and measurements along a particular symmetry line in k space with a constant parallel component $k_i^{\parallel}$ of the wave vector.[2–5,7]

The determination of surface-state energy dispersion is relatively simple once the emission from surface states is identified, because the perpendicular component $k_i^{\perp}$ of the wave vector to the surface is undefined for surface states and the energy dispersion is reduced to a function of $k_i^{\parallel}$. This component can be determined from the conservation of energy and the conservation of $\mathbf{k}$ in the direction parallel to the surface given a specular surface. On the other hand, the determination of the energy dispersion $E_i(\mathbf{k}_i)$ for bulk valence bands is highly model dependent,[8] due to the nonconservation of $\mathbf{k}$ in the direction perpendicular to the surface when electrons cross the surface during the photoemission process.[9] The problem is associated with the determination of $k_i^{\perp}$ from the wave vector of the electron detected outside the solid $\mathbf{k}_{\text{outside}}$, but the difficulty can be removed by assuming a direct-transition model within the semiclassical "three-step" model of photoemission,[10] with some knowledge of the final-state energy dispersion $E_f(\mathbf{k}_f)$. In this regard, a free-electron-like final-state (FELFS) model has been employed successfully for energies down to about 16 eV above the valence-band maximum for GaAs(001) surfaces.[2,3] Final-state bands calculated by an empirical-pseudopotential method have also been used recently for interpretation of normal-emission spectra for photon energies between 10 and 34 eV from GaAs(001) surfaces.[7] The experimental features observed at about the X_3 critical point (binding energy -6.6 eV, photon energies between 16 and 30 eV) with no significant $k^{\perp}$ dependence were found, in particular, to be mainly bulk derived and can be explained as k-conserving transitions from valence-band states near X_3 to several final states.

Although some results have been obtained concerning the bulk- and surface-state band structure from the previous studies, these studies were, however, confined to normal emission ($k_i^{\parallel}=0$) or to data related to a particular constant-$k_i^{\parallel}$ line and our understanding of the electronic structure of (001) surfaces of GaAs is still limited.[1] Features observed in off-normal-emission spectra may also give rise to features observed in the normal direction. Information from off-normal-emission spectra should therefore be fully considered in order to correctly identify the origin of observed transitions in the normal-emission spectra.

Structure plots have proved to be very useful for analyzing photoemission data. Two types of structure

plots showing peak energies versus photon energy and polar emission angle, respectively, have been used in this paper. Experimental points have been compared with theoretical transition lines generated under a direct-transition model. The observed bulk-related experimental features are interpreted within the semiclassical three-step model. The theoretical transition lines were constructed using initial-state bands calculated by a linear-muffin-tin-orbital (LMTO) program of Christensen[11] and a free-electron-like final-state model for the final-state-band dispersion. In the following sections, experimental details are presented, followed by a discussion and an evaluation of the experimental results using the above structure plots.

II. EXPERIMENT

The GaAs(001) samples were grown on semi-insulating GaAs(001) substrates in a modified Varian 360 molecular-beam epitaxy (MBE) system at a temperature of 600 °C. Following the growth, and before removal from the UHV growth chamber, a thick amorphous layer of arsenic was deposited to protect the sample surface. This capping was achieved by cooling the sample holder via a liquid-nitrogen cold finger and then leaving the sample at an As background pressure of 4×10^{-5} Torr for 1–2 h. This technique has previously been used successfully to preserve UHV-grown GaAs surfaces during sample transfer to the synchrotron radiation source.[12]

The samples were then heated to a temperature around 300 °C in a preparation tank to remove the As amorphous overlayer before being transferred under UHV to the analyzer chamber for the photoemission measurements. The heating time normally lasted about 1 h. A highly reflecting surface, characteristic of the MBE-grown material, was obtained after such preparation. The surface cleanliness was confirmed both by a clear 1×1 low-energy electron diffraction (LEED) pattern indicative of an As-terminated surface[13] and by photoemission spectra taken at a photon energy around 30 eV where the electron mean free path is small and the spectra are particularly sensitive to contamination.

With the working pressure maintained normally at 2×10^{-10} Torr, angle-resolved photoemission spectra were acquired in the photon-energy range of 10–70 eV using the TGM-4 beamline at Berliner Elektronenspeicherring-Gesellschaft für Synchrotronstrahlung m.b.H. (BESSY), Berlin. The electron-energy analyzer used was of toroidal geometry[14] using position-sensitive detection technology to render it multidetecting in terms of the polar-emission angle of photoelectrons. All data acquired were consequently angle resolved over the full 180° range, the angular resolution being close to ±1.0°. The azimuthal angle was defined to within ±1°. The characteristics of the monochromator at the beamline may be found in Ref. 15. The widths of the entrance and exit slits of the monochromator were always set to maintain a theoretical resolution of 0.1 eV or better during the measurements: together with the analyzer, the overall energy resolution in the measurements was 0.2 eV. In Fig. 1 we show the experimental geometry and the measurement plane in k space. P-polarized light was incident at 45° to the surface normal in the measurement plane, the azimuthal direction being the [100] symmetry line.

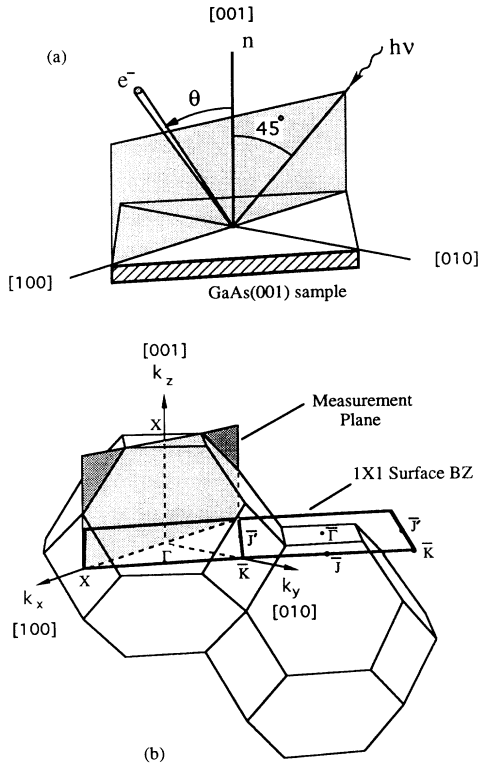

FIG. 1. (a) The experimental geometry and (b) the face-centered-cubic Brillouin zone in relation to the 1×1 surface Brillouin zone. The measurement plane is taken along the [100] azimuth.

Photon-energy calibration was performed by taking Ga-3d core-line measurements at each photon energy using first-, second-, and third-order light wherever possible. The apparent binding energy of the core line was determined precisely by fitting the core-line spectra using Gaussian profiles including a constant spin-orbit splitting of 0.46 eV, and the nominal photon energy adjusted accordingly.

III. RESULTS AND DISCUSSION

A large number of angle-resolved photoemission spectra were collected on the GaAs(001) sample with the present experimental geometry. Each data set contains information regarding the emission intensity as a function of both the initial energy E_i and the emission (polar) angle θ (from $-90°$ to $+90°$) for a specific excitation energy (photon energy). A normal-emission spectrum can be extracted from such a data set and a selection of normal-emission spectra covering the photon-energy range 10.2–50.5 eV is shown in Fig. 2. The energy is shown relative to the valence-band maximum (VBM), which was identified as the peak with lowest binding energy (observed in the photon-energy region of 10–15 eV).

In order to analyze the normal-emission spectra, a

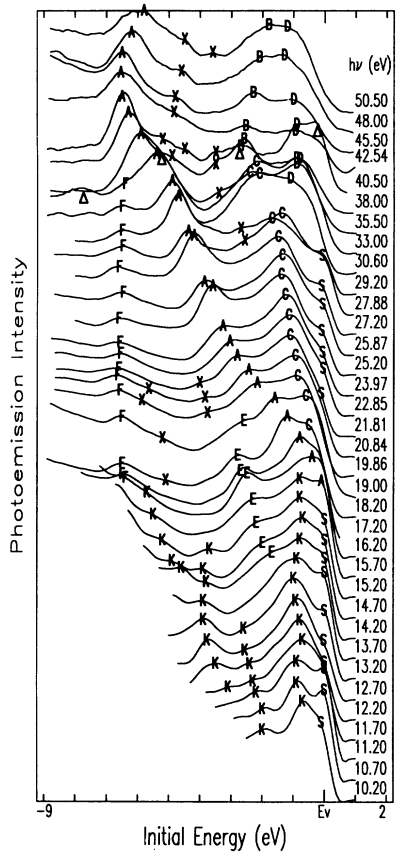

FIG. 2. Normal-emission spectra for photon energies from 10.2 to 50.5 eV for GaAs(001)-1×1 surface. Detected peaks are marked by letter symbols relating to their assignments to various transitions (refer to the text). The As-3*d* core-line emissions excited by the second-order light from the monochromator are indicated by open triangles △.

structure plot of initial-energy E_i v's photon energy $h\nu$ is employed. This method has been used previously by Williams *et al.*[16] for the interpretation of photoemission data taken from the (110) surface of III–V compound semiconductors and by Olde *et al.*[7] for a GaAs(001)-$c(4\times4)$ surface. Basically, the structure plot consists of experimental points taken from peaks in the normal-emission spectra of Fig. 2 and of theoretical transition lines generated according to a theoretical model. Readers are referred to Refs. 7 and 16 for detailed descriptions of the construction of the theoretical transition lines.

On the other hand, electronic structure observed at a single photon energy may be presented as a plot of E_i v's θ with marked peak positions determined from energy distribution curves (EDC's) at different polar-emission angles. An $E_i(\theta)$-structure plot is employed here to study such data with theoretical lines being generated from a free-electron-like final-state model in conjunction with the LMTO-calculated valence bands. Bringans and Bachrach[17] have used this structure plot in a slightly different form (E_i v's $k^{\parallel}$) for a GaAs(001)-$c(4\times4)$ surface. In the following, a brief description of the construction of these theoretical $E_i(\theta)$ lines is given.

A. Structure Plot of E_i v's θ

The major difference between the structure plot of E_i v's θ and the structure plot for normal emission is that emission is no longer limited to a particular symmetry line in k space, but involves transitions that span $(k^{\parallel},k^{\perp})$ surfaces. Under the three-step model, a direct transition implies that the momentum of electrons inside the solid is conserved modulo a bulk reciprocal-lattice vector $\mathbf{G}$ in the interband transition between initial-state band $E_i(\mathbf{k}_i)$ and final-state band $E_f(\mathbf{k}_f)$. If the energy surfaces $E_i(k_i^{\parallel},k_i^{\perp})$ and $E_j(k_f^{\parallel},k_f^{\perp})$ are known, possible transitions with excitation energy of $h\nu$ (photon energy) can then be predicted by calculating the constant energy difference curves (CEDC's) (Ref. 18) between them from the following equation:

$$\Delta_{fi}(k^{\parallel},k^{\perp})=E_f(k^{\parallel},k^{\perp})-E_i(k^{\parallel},k^{\perp})-h\nu=0\ . \tag{1}$$

Here, because of the momentum conservation inside the crystal, $\mathbf{k}_i$ and $\mathbf{k}_f$ have not been distinguished and have been referred to as $\mathbf{k}$, and therefore $k_i^{\parallel}=k_f^{\parallel}=k^{\parallel}$ and $k_i^{\perp}=k_f^{\perp}=k^{\perp}$.

Since momentum parallel to the surface is also conserved in the process of photoemission from specular surfaces, the polar angle θ is related to $k^{\parallel}$ by

$$\mathbf{k}^{\parallel}=\mathbf{k}^{\parallel}_{\text{outside}}+\mathbf{g}=\frac{\sqrt{2mE_{\text{kin}}}}{\hbar}\sin\theta\frac{\mathbf{k}^{\parallel}}{|\mathbf{k}^{\parallel}|}+\mathbf{g}\ , \tag{2}$$

where, $\mathbf{g}$ is a surface reciprocal-lattice vector and E_{kin} is the kinetic energy of the electrons with respect to the vacuum level E_{vac} of the spectrometer and can be determined from the following energy conservation relation once E_{vac} is determined from experiment:

$$E_{\text{kin}}=h\nu+E_i-E_{\text{vac}}\ ; \tag{3}$$

and where E_{vac} is measured from the valence-band maximum.

In this paper, initial-state energy surfaces are calculated by the LMTO program mentioned earlier, and labeled by band numbers counting from the lowest valence band. The calculations were performed on a grid of 21×52 energy points spanning a rectangular portion of the k plane concerned within the face-centered-cubic (fcc) Brillouin zone (BZ). For the measurement plane chosen for this work, for example, the calculation boundaries are the $\Gamma X(k^{\perp})$-$\Gamma X(k^{\parallel})$ lines (see Fig. 1).

Final-state energy surfaces are calculated using the free-electron-like parabolic surface given by

$$E_f(k^{\parallel},k^{\perp})=\frac{\hbar^2}{2m}(\mathbf{k}^{\perp}+\mathbf{k}^{\parallel}+\mathbf{G})^2+E_0\ , \tag{4}$$

where $|\mathbf{k}^{\parallel}|=k^{\parallel}$, $|\mathbf{k}^{\perp}|=k^{\perp}$, $0\le k^{\parallel},k^{\perp}\le 2\pi/a$ for the ΓX-ΓX plane (reduced-zone scheme), and where a is the lattice constant of GaAs, E_0 is the inner potential with respect to the VBM, and $\mathbf{G}=(2\pi/a)(l,m,n)$ is a reciprocal vector of the bulk crystal. Different energy surfaces are labeled by the associated $\mathbf{G}$ vector. Those with $(l,m,n)=(0,0,n)$, where $n=0,\pm2,\pm4,\ldots$, being perpendicular to the surface, are primary-cone surfaces with respect to the normal-emission direction.[19] Others are

referred to as secondary-cone surfaces by Himpsel.[20] This terminology is commonly used now in the literature because normal-emission studies (e.g., Refs. 2 and 3) have found that interband transitions associated with **G** not perpendicular to the surface are much weaker than those associated with perpendicular **G** vectors. This terminology will also be used in this paper, although the secondary cones referred to here would be referred to as primary cones associated with each **G** vector according to Mahan.[19]

Once the CEDC's are obtained from Eq. (1), they can be projected onto the $E_i(\theta)$-structure plot using Eqs. (2) and (3), for comparison with experiment. For simplicity, no restriction on the transitions relating to the symmetry-selection rules for p-polarized light are considered in this study in the calculation of the CEDC's.

Surface umklapp processes occur only when excited electrons cross the surface under the three-step model and the surface reciprocal **g** vector is not considered in the optical (interband) transition.[21] This is described in Eq. (2) with $\mathbf{g}\neq 0$. Under the present experimental geometry (see Fig. 1), $\mathbf{k}^{\parallel}_{\text{outside}}$ has to be within the measurement plane (i.e., the ΓX-ΓX plane) for the emitted electrons to be detected by the spectrometer. The associated interband transitions are thus confined to the ΓX-ΓX plane for $\mathbf{g}=0$, or to a k plane parallel to and separated from the ΓX-ΓX plane by the **g** vector, should the detected electrons have been involved in surface umklapp processes. For the present 1×1 unreconstructed surface, however, it can be shown (see the Appendix) that surface umklapp processes involving any of the available surface **g** vectors do not produce structures [in $E_i(\theta)$ plots] different from those being produced by direct transitions within the ΓX-ΓX plane. Therefore, surface umklapp processes are not considered in the following discussion, although it is likely that they also contribute to the observed structures.

Direct transitions from surface states have also been considered in this study and have been compared with theoretical calculations for a GaAs(001) As-terminated surface by Pollmann and Pantelides.[22] They used an empirical tight-binding approximation to describe the bulk material and solved the surface problem via a Green's-function formulation of scattering theory. Only the dangling-bond band in the fundamental gap along the $\bar{\Gamma}\bar{K}$ direction of the 1×1 surface BZ is relevant here, since there is no obvious mechanism available for other occupied surface states at energies higher than -8 eV to be seen in the measurement plane. The mapping of the surface-state band $E_i(k_i^{\parallel})$ onto the $E_i(\theta)$-structure plot is straightforward and can be performed using Eq. (2) with $\mathbf{g}=0$ and Eq. (3). We now return to the interpretation of the experimental data.

B. Normal emission

To begin with, let us first consider normal-emission spectra. Experimental points (detected peaks) from the normal-emission spectra of Fig. 2 are shown in Fig. 3 as a plot of initial energy E_i versus photon energy $h\nu$. Peaks from core-level emission excited by higher-order light have been eliminated from the plot. For convenience in discussion, experimental points have been divided into several groups and labeled with letter symbols relating to their assignment to various transitions. The intensity of peaks can be inferred from Fig. 2 where the corresponding peaks have been marked.

Theoretical transition lines in Fig. 3 were generated using the LMTO-calculated valence bands 2, 3, and 4 along the $\Gamma\Delta X$ line in the ΓX-ΓX plane and the FELFS's given by Eq. (4) with $k^{\parallel}=0$. Thick solid lines are primary-cone transitions, other line styles are secondary-cone transitions, the (lmn) indices for the associated **G** vectors being $(\bar{1}11)$, $(\bar{1}1\bar{3})$, and $(\bar{1}13)$ for dashed lines, (020), $(02\bar{2})$, and (022) for dash-dotted lines, and $(\bar{2}20)$, $(\bar{2}2\bar{2})$, and $(\bar{2}22)$ for dotted lines. The best fit between the experimental points as a whole and the theoretical transition lines is obtained with an inner potential $E_0=-7.0$ eV. Other values of E_0 have been used for GaAs(001) surfaces in the literature: Olde *et al.*[7] reported a value of -6.6 eV, whereas Chiang *et al.*[2] and Larsen *et al.*[3] used a value of -7.7 eV for the inner potential. In the papers of Chiang *et al.* and Larsen *et al.*, the VBM was chosen at the onset of the spectra, while in our case, the VBM is chosen at the peak position where emission from the Γ_{15}^{v} point is identified. Peak positions have traditionally been used to map band structures and for comparison with theoretical

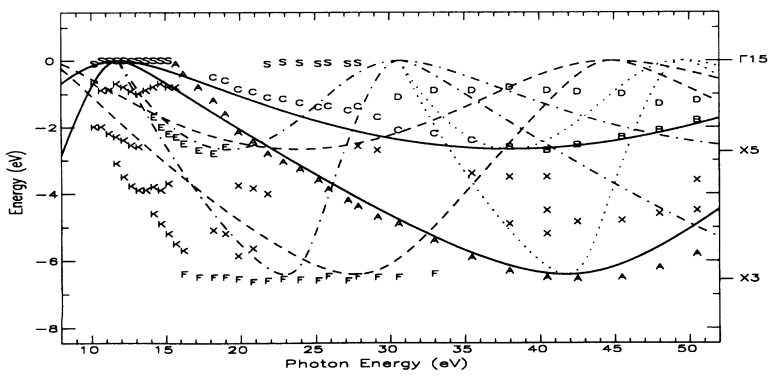

FIG. 3. Structure plot for photoelectron normal-emission data from a GaAs(001)-1×1 surface. Theoretical transition lines are generated using LMTO-calculated valence bands Δ_1, $\Delta_{3,4}$ along the $\Gamma\Delta X$ direction in the ΓX-ΓX plane together with free-electron-like final states using an inner potential $E_0=-7.0$ eV. Thick solid lines are primary-cone transitions; other line styles are secondary-cone transitions. The energy is with respect to the valence-band maximum.

calculations in previous photoemission experiments. To be consistent, we consider that the peak position should also be used for the determination of the VBM location. The difference in energy from the onset of the spectra to this peak position is 0.45 eV from our data. Our value of E_0 is close to that of Chiang *et al.* and Larsen *et al.* if this difference is allowed for.

From Fig. 3, the two strongest experimental features, namely those with letter symbol A in the photon-energy range of 19–43 eV and those labeled B, are seen to follow the locus of primary-cone transition lines. The fitting in energy is within experimental error. They are, therefore, identified as primary-cone transitions from valence bands Δ_1 (A) and $\Delta_{3,4}$ (B) (corresponding to the LMTO band 2 and the degenerate bands 3 and 4, respectively), in agreement with previous work.[2,3,7,23] The Δ_1-band emission starts to deviate in energy from the theoretical transition line at $h\nu=19$ eV and reaches the Γ_{15} point at $h\nu\simeq 15.5$ eV, approximately 4 eV higher than the position predicted by the FELFS model. This can be accounted for as a deviation of the real final-state dispersion from the free-electron-like parabola near the Brillouin-zone center. Assuming that the LMTO initial states are of the correct shape, a real final-state band can be derived by first mapping the A experimental points onto the LMTO initial band 2 (To determine the $k^{\perp}$ of the experimental points from the initial energy, the theoretical bandwidth has been adjusted to fit the experimentally determined critical-point energy $E^v_{X_3}=-6.54$ eV) and then shifting the experimental point vertically by the corresponding photon energy. The resulting final-state dispersion is shown in Fig. 4. A similar result was also obtained by Middelmann *et al.*[24] for α-Sn.

Transitions from the $\Delta_{3,4}$ band, occurring at photon energies between 18 and 36 eV and shown by C in Fig. 3, do not follow the primary-cone transition lines. This is in contrast to the work by Chiang *et al.*[2] and by Larsen *et al.*[3] where they reported a good fit for these transitions. The maximum deviation (about 0.8 eV) is seen at $h\nu=28$ eV in our data, from where another structure (labeled D) is developed above the primary-cone transitions from the $\Delta_{3,4}$ band. No theoretical transition lines fit these transitions in Fig. 3, although the secondary-cone transition lines go through this region. Since a convincing explanation of this inconsistency involves the study of the off-normal-emission data, we leave it to Sec. III C.

There are two features in Fig. 3 that we identify as transitions involving secondary cones. The first set, labeled E, can be identified as emission from the $\Delta_{3,4}$ band to the (020) band. Stronger emission is observed for these transitions as the binding energy of the X_5 point ($E^v_{X_5}=-2.74$ eV from our experiment) is approached (see Fig. 2), although emission cannot be identified after 19 eV. The second set, labeled by letter symbol F, is associated with transitions from the region of high density of states near the X_3 point to the lifetime-broadened secondary-cone final states. This interpretation will be further discussed in the off-normal emission data presented later in Sec. III C. Other features left unexplained in the normal-emission spectra are generally weak and will be examined in conjunction with the off-normal-emission spectra below.

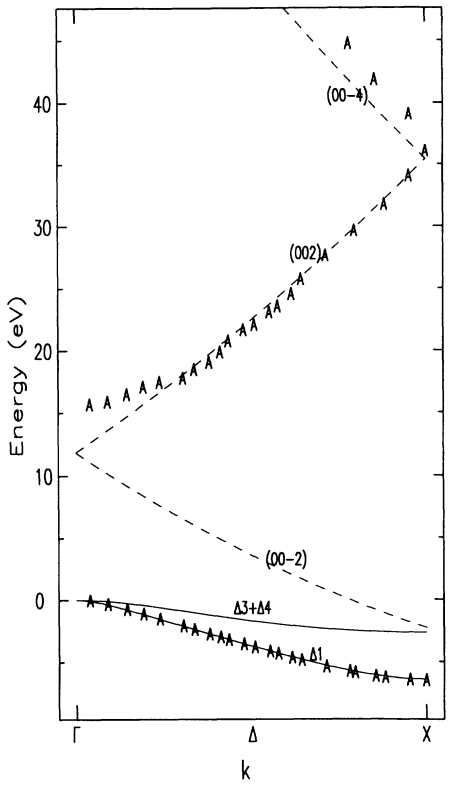

FIG. 4. Experimental band structure for the Δ_1 band along the $\Gamma\Delta X$ direction and the corresponding experimental final-state band determined as described in the text. The dashed lines are the primary cones of the free-electron-like final states with inner potential $E_0=-7.0$ eV.

C. Off-normal emission

Off-normal-emission spectra, though less frequently studied in the past, contain much information. Figure 5 shows a selection of structure plots of the $E_i(\theta)$ type. Experimental peaks determined from EDC's at different polar angles are shown using letter symbols inherited from the normal-emission study. Two different types of theoretical transition lines have been generated in Fig. 5. The cross-hair symbols ⊕ represent direct transitions from the dangling-bond surface band of the calculations of Pollmann and Pantelides.[22] The solid lines represent direct transitions from the bulk bands to the FELFS primary-cone final states. They are generated by calculating the CEDC's between the LMTO-valence-band surfaces 2, 3, and 4 in the ΓX-ΓX plane and the primary-cone free-electron-like final-state parabola [Eq. (4)] using an inner potential of $E_0=-7.0$ eV relative to the VBM, the associated **G** vectors being $(00\bar{2})$, (002), and $(00\bar{4})$.

For $h\nu<16$ eV, off-normal-emission spectra are very similar in general shape and can be represented by the spectrum taken at a photon energy of 12.70 eV [Fig. 5(a)]. No obvious structures in the plot can be attributed to primary-cone transitions, suggesting, as expected, that

the FELFS model is not applicable for direct transitions in this energy region. However, this does not mean that no true direct bulk transitions occur in this energy region. In fact, the strong emission, labeled K, observed at $E_i \simeq -1.0$ eV over the full polar-angle range is probably due to direct transitions from bulk valence bands to the real conduction bands. This structure shows significant dispersion in normal emission (see Fig. 3) and is therefore not emission from a surface state. This argument can also be applied to the other strong emissions in Fig. 5(a), also labeled K, observed at $E_i \simeq -2.5$ and -3.7 eV for $-20° < \theta < +20°$. On the other hand, the emissions with $\theta < -20°$ and $\theta > +20°$ and labeled by E, continuing from the K feature at $E_i \simeq -3.7$ eV, are of a different nature. They are associated with secondary-cone transitions and will be considered later.

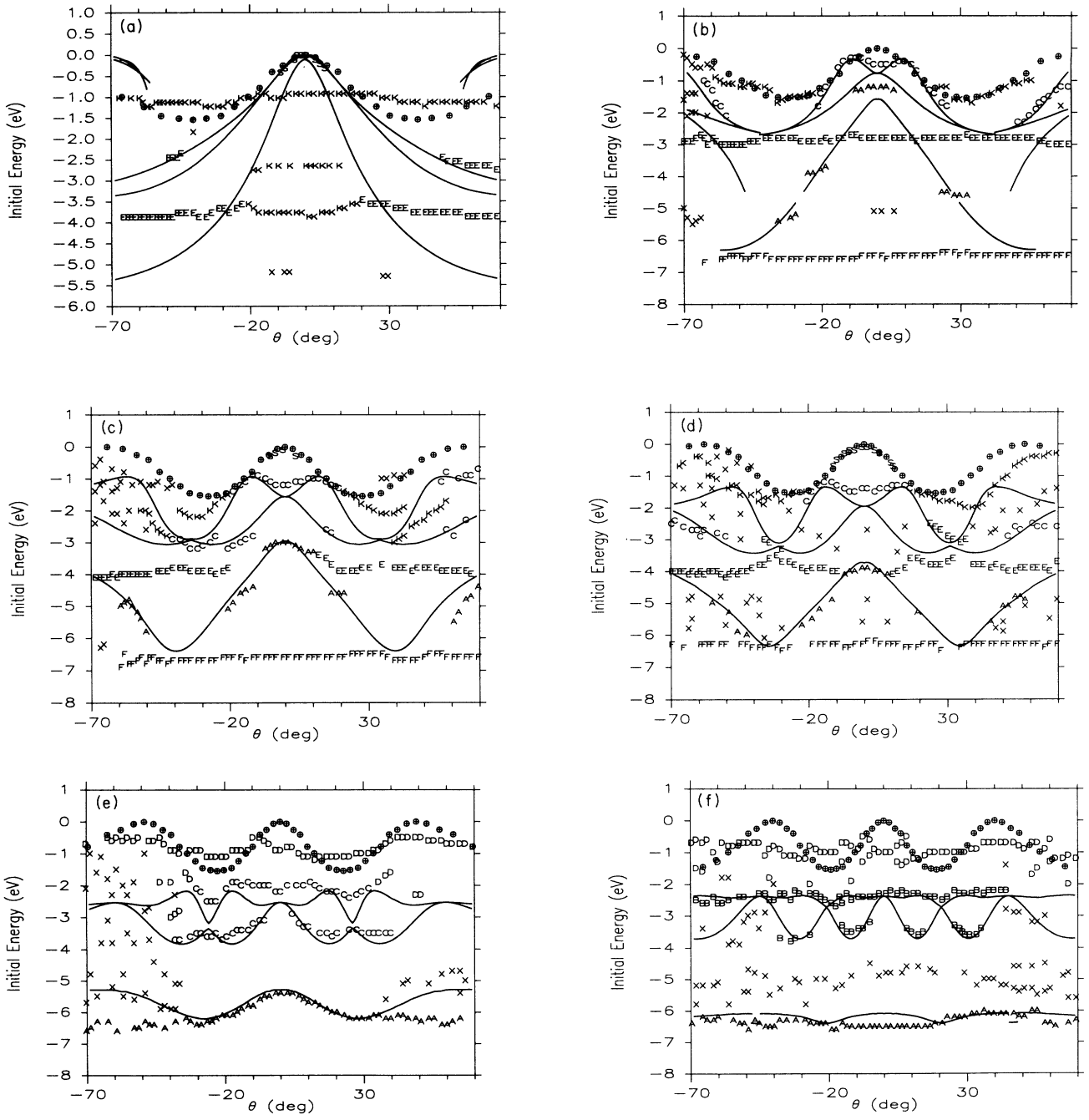

FIG. 5. Structure plots of E_i v's θ. Letter symbols mark the detected peak positions in the spectra. Details of the construction of the theoretical transition lines are given in the text. The initial energy is relative to the valence-band maximum. The excitation energy for each structure plot is as follows: (a) 12.70 eV, (b) 18.20 eV, (c) 23.20 eV, (d) 26.20 eV, (e) 33.00 eV, and (f) 45.50 eV.

Regarding the crescent of emissions, labeled S, observed at the valence-band maximum for $-10° < \theta < +10°$ in Fig. 5(a), this can be identified as direct transitions from the dangling-bond state as calculated by Pollmann and Pantelides,[22] but contributions from the bulk-band primary-cone transition may also be present because both theoretical lines fit this experimental feature. Referring to the normal-emission-structure plot Fig. 3, a dispersionless feature with S is observed at the valence-band maximum for photon energies from 10 to 16 eV. This feature continues for photon energies from 22 to 29 eV and the associated off-normal emission can be seen in Figs. 5(c) and 5(d) within $-10° < \theta < +10°$. The emission intensity of the S feature in the normal-emission direction is rather consistent, as is evident from Fig. 2, except at a photon energy of 10.70 eV, where we observe strong emission. According to a recent study on the GaAs(110) surface using angle-resolved constant-initial-state spectroscopy,[25] it is found that the conduction-band energies at the Γ point (relative to the VBM) in the energy region of 10–16 eV are 10.72, 12.60, and 15.20 eV. Our normal-emission study above shows a possible Γ-point energy at 15.5 eV. The emission at the VBM for $h\nu = 10.70$ eV suggests further that there exist contributions from both the surface state and the direct bulk transition for this excitation energy, and thus confirms the results of Ref. 25.

We now move on to discuss the off-normal-emission spectra taken for photon energies greater than 16 eV. To begin with, we concentrate on the interpretation of the feature C. As can be seen from Figs. 5(b) and 5(c), strong transitions within $-20° < \theta < +20°$ near the VBM, i.e., the feature C, mimic the shape of the theoretical lines for primary-cone direct transitions from the LMTO band 4, but the energy at $\theta = 0$ is on average 0.35 eV higher than the position predicted by the free-electron-like final-state model for photon energies from 16–24 eV. Greater deviations from the primary-cone transition lines are seen [see Figs. 5(d) and 5(e)] for photon energies greater than 25 eV for this transition, leading to the result that the feature C in the normal-emission direction cannot be accounted for as direct transitions from $\Delta_{3,4}$ bands to the primary cone of the free-electron-like final states.

Since there is also no contribution from secondary-cone transitions in normal emission for photon energies from 16 to 24 eV for the feature C, as is evident from Fig. 3, the feature C must be due to direct interband transitions. A theoretical study that used a time-reversed LEED state to perform one-step photoemission calculations[26] showed that the final state for allowed direct transitions from the degenerate $\Delta_{3,4}$ bands in normal emission is not free-electron-like, leading to low transition probability. The photoemission intensity from the $\Delta_{3,4}$ band was also predicted to be weaker than that from the Δ_1 band. On the other hand, two strong emissions are present in off-normal-emission spectra as can be seen from Figs. 5(b) and 5(c) at polar angles close to $\pm 10°$. Our studies[27] have found that these two strong transitions can dominate the spectrum in this energy region due to momentum broadening and thus prevent the observation of the direct transition from the $\Delta_{3,4}$ band in the normal-emission direction. The observed C feature in this photon-energy range is, therefore, a combination of those two effects.

Regarding the good fit reported for the $\Delta_{3,4}$-band transitions in the normal-emission studies of Chiang *et al.*[2] and of Larsen *et al.*,[3] we believe this was achieved partly by their use of empirical tight-binding valence bands with parameters adjusted to fit the experimentally determined critical-point energies. A better degree of fit can also be achieved by a different choice of the inner potential E_0 if a limited photon-energy range (20–32 eV in the work of Larsen *et al.*) is used. Furthermore, deviations of up to approximately 0.5 eV were observed between the experimental points and the theoretical line for $\Delta_{3,4}$ band transitions in the work of Chiang *et al.* (Fig. 6 of Ref. 2).

The influence of the normal-emission spectra from the nearby two strong peaks mentioned above due to momentum broadening weakens as the photon energy increases and as their separation in polar angle increases, whereas transitions to secondary cones appear in normal emission in this energy region [see Figs. 3, and Figs. 6(e) and 6(f) presented later]. These extra transitions exist at higher photon energies and could probably contribute to the feature D observed in the normal-emission spectra in Fig. 3. Due to the large number of different secondary-cone transition lines going through this region, it is not practicable to analyze the source of these transitions in detail and we will not discuss the D feature further in the present paper.

Beyond the polar-angle range of $-20° < \theta < +20°$ for photon energies less than 30 eV, there exist some strong transitions, labeled K, arising from LMTO band 4 as shown in Figs. 5(c) and 5(d). They follow neither the primary-cone transition lines nor the theoretical surface-state transitions. Examination of these experimental points along other nonzero constant-$k^{\parallel}$ lines also shows significant dispersion. They are, therefore, due to true bulk transitions.

Emission from LMTO bands 3 and 4 seen in the spectra taken at photon energies greater than 35 eV, i.e., the B feature, show good agreement with the theoretical transition lines and can be seen in Fig. 5(f), confirming the conclusion concerning their origin made in the normal-emission study above. Direct transitions from LMTO band 3 are not generally seen near the normal-emission direction; only a few transitions in off-normal-emission directions can be identified as direct transitions from this band. This fact could not be determined from the normal-emission study alone due to the degeneracy of bands 3 and 4 in the $\Gamma\Delta X$ direction. For LMTO band 2, direct transitions (the A feature) for excitation energies from 20 to 43 eV mimic the shape of the primary-cone transition line in the off-normal-emission direction and the deviation in energy is within experimental error. Figure 5(e) shows the situation where the transitions are excited by a photon energy of 33.0 eV. The angle range of this agreement for feature A decreases at lower photon energies as can be seen in Figs. 5(c) and 5(d), and beyond this angle range, the spectra are dominated by transitions arising from secondary-cone transitions [see feature E in Figs. 6(c) and 6(d) presented later]. For excitation ener-

gies higher than 43 eV, the direct transition from LMTO band 2 does not follow the dispersion predicted by the free-electron-like final-state model within $-20° < \theta < +20°$ and the experimental features become very flat in the off-normal direction, as shown in Fig. 5(f). Given the success of the FELFS model in the photon-energy range of 20–43 eV, this behavior is unexpected.

We now consider the secondary-cone transitions in the off-normal-emission spectra. The corresponding theoretical transition lines are presented in Fig. 6 with the same set of experimental data in Fig. 5 for comparison. The theoretical transition lines are generated using the LMTO-calculated valence bands 2, 3, and 4 in the ΓX-ΓX plane and the FELFS secondary cones with indices $(\bar{1}1\bar{1})$, $(\bar{1}11)$, and $(\bar{1}1\bar{3})$ for solid lines, and indices (020), $(02\bar{2})$, and (022) for dashed lines. Transition lines to the third secondary cones with indices $(\bar{2}20)$, $(\bar{2}2\bar{2})$, and $(\bar{2}22)$ are not presented here for clarity, since they mainly go through regions containing the D experimental feature.

We first consider the situation, represented by Fig. 6(a),

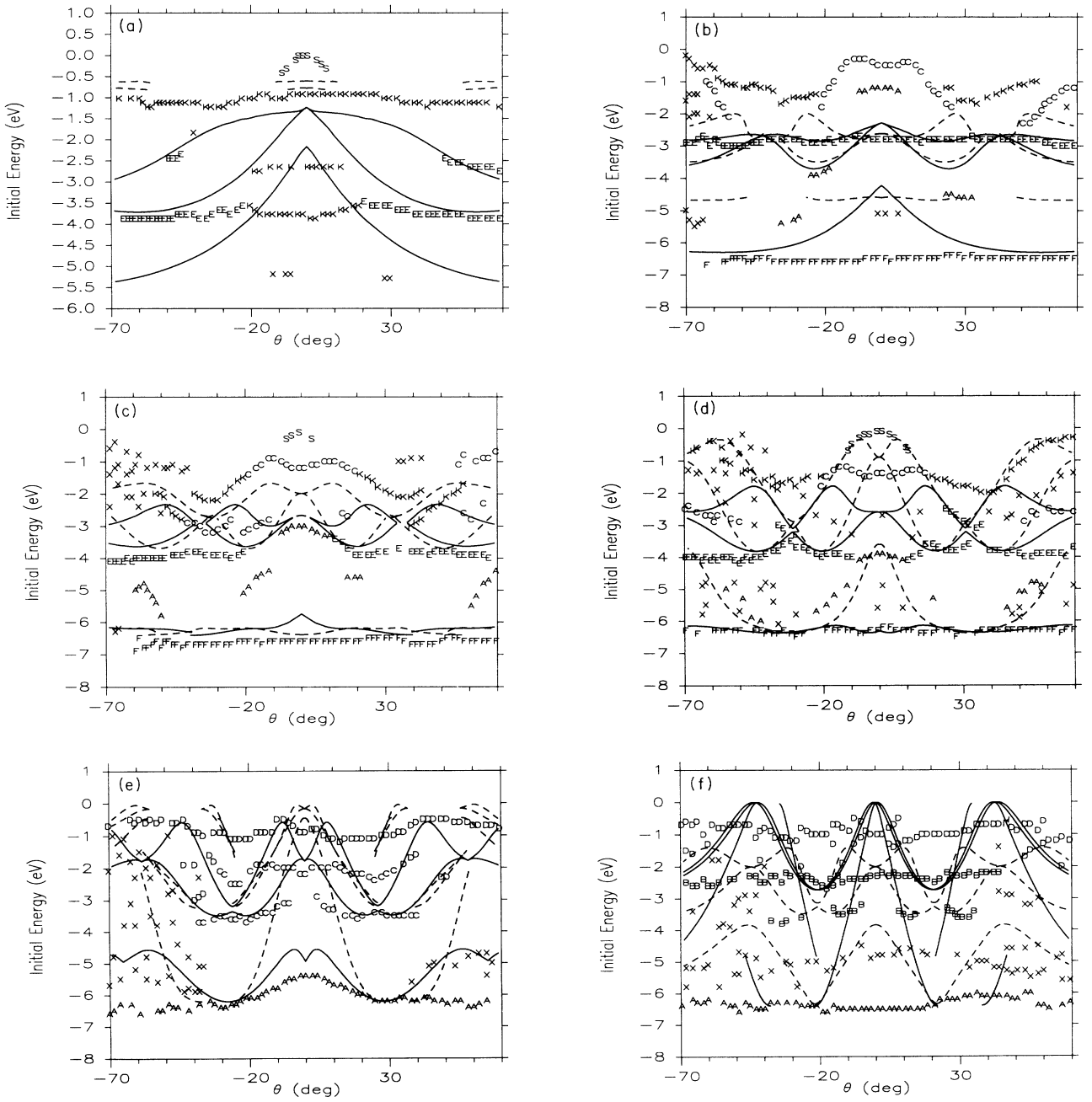

FIG. 6. Structure plots of E_i v's θ for secondary-cone transitions. Details of the construction of the theoretical transition lines are given in the text. The excitation energy for each structure plot is as follows: (a) 12.70 eV, (b) 18.20 eV, (c) 23.20 eV, (d) 26.20 eV, (e) 33.00 eV, and (f) 45.50 eV.

for $h\nu < 16$ eV. The experimental feature E is seen to follow the solid lines for $\theta < -40°$ and $\theta > +40°$ but starts to deviate in energy up to approximately 1 eV from the theoretical transition lines toward smaller polar-emission angles, suggesting that the E feature is probably due to the secondary-cone transitions. The good fit for this feature in the polar-angle range $\theta < -40°$ and $\theta > +40°$ indicates that the FELFS's are a good representation of the real final states corresponding to the secondary cones in this energy region.

Regarding the situation for $h\nu > 16$ eV, it has been pointed out in the normal-emission study presented above that there are two main features in the normal-emission spectra that can be identified as secondary-cone transitions from around the X-critical points in the bulk bands. Correspondingly, feature E can be seen in Fig. 6(b) and feature F in Figs. 6(b)–6(d). Feature E can also be seen in Figs. 6(c) and 6(d) in the off-normal direction. In particular, the E feature in Fig. 6(b) at $E_i \simeq -3.0$ eV follows the secondary cone with indices (020) and $(02\bar{2})$ (dashed lines) in the region $-10° < \theta < +10°$ and the other secondary cone with index $(\bar{1}1\bar{1})$ (solid lines) beyond this polar-angle region, forming a relatively flat feature running through the whole polar-angle range. This behavior is seen in all the off-normal-emission spectra corresponding to the identification of the E features in the normal-emission spectra (Fig. 3) as being due to secondary-cone emission from the $\Delta_{3,4}$ band for photon energies from 14–19 eV, confirming the conclusion made in the normal-emission study.

At higher photon energies, the E feature [see Figs. 6(c) and 6(d)] is also dispersionless at the energy appropriate to the flat region of energy surfaces toward glancing emission angles. Although the theoretical transition lines do not fit the experimental points, it is likely that they are still direct transitions in nature and are a combination of the final-state-broadening effect and the high density of states associated with the flat region of the bands. This is also the case for F feature seen in Figs. 6(b)–6(d). The similarity between the experimental points and the theoretical transition lines for the F feature in Figs. 6(c) and 6(d) indicates that they are due to the corresponding secondary-cone transitions. The observed deviations in energy from the theoretical transition lines in the normal-emission study for the F feature may be accounted for by the final state-broadening effect at high photon energies and by the inadequacy of the free-electron-like final states at low photon energies.

It can therefore be concluded that umklapp transitions involving bulk- and/or surface-reciprocal vectors generally occur around critical points (or flat regions of the energy surfaces in off-normal emissions) with an associated high density of states and exhibit little dispersion along the $k^{\parallel}$ direction. With the final-state lifetime broadening becoming more prominent as the excitation energy increases, these transitions also show little dispersion along the $k^{\perp}$ direction. They are k-conserving direct transitions in nature and, therefore, should not be described as one-dimensional density-of-states effects, which are very much a concept inherited from the indirect transition model of photoemission.

IV. SUMMARY

Angle-resolved photoemission experiments have been performed on the As-terminated GaAs(001)-1×1 surface grown by molecular-beam epitaxy. The structure $E_i(k_i^{\parallel}, k_i^{\perp})$ observed in the spectra has been explained in detail using a free-electron-like final-state model in conjunction with LMTO-calculated initial-state bands. Experimental features from surface-states and bulk bands have been identified. Experimental valence-band structures could be mapped based on these results, although this would simply confirm the validity of the LMTO bands. From the discussion and results presented in this paper, it can be seen that the free-electron-like final-state model has mixed success for the GaAs(001)-1×1 surface over the full range of photon energies used. No general limit, however, can be established as to the lowest final-state energy for which the model is useful for predicting the initial-state band dispersion in k space. Even in the case where the theoretical transition lines generated based on this model mimic the shape of the experimental dispersion, deviations in energy were observed up to 0.35 eV in normal emission and up to about 1 eV in off-normal emission. For primary-cone direct transitions in the normal direction, the limit is estimated to be around $h\nu = 20$ eV. This does not ensure, however, that the model is equally applicable to other emission directions. It is also evident that photoemission is a very complicated process and that an experimental feature may contain contributions from a number of different sources. Furthermore, one-dimensional density-of-states effects may be described as direct transitions involving bulk and/or surface umklapp processes from critical points or flat regions of the initial energy surfaces where there is a high density of states.

ACKNOWLEDGMENTS

This work has been supported by the Australian Research Grants Scheme, by the Australian-German Scientific and Technical agreement, and by the Bundesministerium für Forschung und Technologie. Thanks are due to the staff, especially W. Braun of BESSY, for their support and hospitality, to G. Kemister for assistance with the LMTO calculations, and to M. Cardona for supporting the collaboration with the Max-Planck-Institut für Festkorperforschung. A.S. and Y.C. wish to thank La Trobe University for financial support.

APPENDIX

With the present 1×1 surface, only the surface reciprocal vector

$$\mathbf{g}_{[\bar{1}10]} = \frac{2\pi}{a}(\bar{1}, 1, 0)$$

is significant for surface umklapp processes; the other symmetrically distinguishable surface reciprocal vector $\mathbf{g}_{[020]}$ is equivalent to a bulk $\mathbf{G}$ vector and will not produce structures different from those being produced by the secondary-cone (bulk umklapp) transitions in Eq. (4).

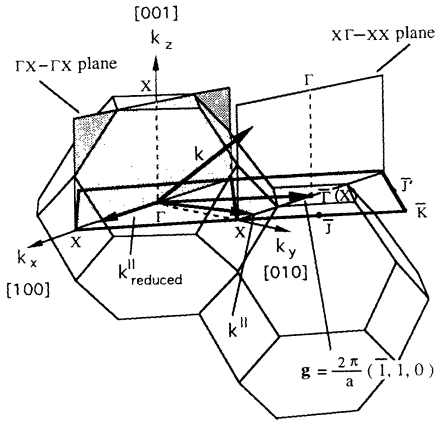

FIG. 7. Illustration of the surface umklapp process involving the surface reciprocal vector $\mathbf{g}=(2\pi/a)(\bar{1},1,0)$ in k space. With the surface umklapp, optical transitions are confined in the $X\Gamma$-XX plane, but the excited electrons can be detected in the ΓX-ΓX plane.

From this consideration, we will consider $\mathbf{g}_{[\bar{1}10]}$ only in the following discussion.

The surface umklapp process involving $\mathbf{g}_{[\bar{1}10]}$ can be illustrated by Fig. 7 where a k plane (the $X\Gamma$-XX plane) parallel to and linked by $\mathbf{g}_{[\bar{1}10]}$ to the ΓX-ΓX plane is shown. Following the discussion in Sec. III A, detected electrons due to this surface umklapp process arise from direct transitions that occur within the $X\Gamma$-XX plane. The corresponding theoretical transition lines can be calculated using initial energy surfaces in the $X\Gamma$-XX plane [calculation boundary lines are $X\Gamma(k^{\perp})$ and $XX(k^{\parallel})$] and final-state surfaces given by Eq. (4) with the $\mathbf{k}$ vector now pointing to the $X\Gamma$-XX plane (i.e., the $\mathbf{k}$ vector is no longer limited to the first BZ).

However, by reducing the $\mathbf{k}^{\parallel}$ to the first BZ using $\mathbf{g}_{[\bar{1}10]}$, one can show that the associated surface umklapp process will not produce any different theoretical structures. In fact, by substituting $\mathbf{k}^{\parallel}=\mathbf{k}^{\parallel}_{reduced}+\mathbf{g}$ into Eq. (4), one obtains

$$E_f(k^{\parallel},k^{\perp})=\frac{\hbar^2}{2m}(\mathbf{k}^{\perp}+\mathbf{k}^{\parallel}_{reduced}+\mathbf{g}+\mathbf{G})^2+E_0 \ . \quad \text{(A1)}$$

For a fcc lattice structure, the (l,m,n) indices for a bulk $\mathbf{G}$ vector must satisfy the following conditions:

$$\begin{aligned} l&=I_1-I_2+I_3 \ , \\ m&=I_1+I_2-I_3 \ , \\ n&=-I_1+I_2+I_3 \ , \end{aligned} \quad \text{(A2)}$$

where I_1, I_2, and I_3 are arbitrary integers. Therefore,

$$\begin{aligned} \mathbf{g}+\mathbf{G}&=\frac{2\pi}{a}(\bar{1},1,0)+\frac{2\pi}{a}(l,m,n) \\ &=\frac{2\pi}{a}(l-1,m+1,n\pm1)\mp\frac{2\pi}{a}(0,0,1) \\ &=\mathbf{G}'\mp\frac{2\pi}{a}(0,0,1) \ , \end{aligned} \quad \text{(A3)}$$

where

$$\mathbf{G}'=\frac{2\pi}{a}(l-1,m+1,n\pm1) \ .$$

By substituting Eq. (A3) into Eq. (A1), we finally obtain

$$E_f(k^{\parallel},k^{\perp})=\frac{\hbar^2}{2m}\left[\left(k^{\perp}\mp\frac{2\pi}{a}\right)\frac{\mathbf{k}^{\perp}}{|\mathbf{k}^{\perp}|}+(\mathbf{k}^{\parallel}_{reduced}+\mathbf{G}')\right]^2+E_0 \ . \quad \text{(A4)}$$

The only difference between Eqs. (4) and (A4) is the shift in $k^{\perp}$ by $2\pi/a$ which effectively exchanges the energy at the Γ point, for example, with that at the X point along the $k^{\perp}$ direction. This is also the only difference between the initial energy surfaces in the ΓX-ΓX and the $X\Gamma$-XX planes. Therefore, the resultant theoretical transition lines will be the same. However, the associated $\mathbf{G}$ vectors [with indices (l,m,n)] in the $X\Gamma$-XX plane will become $\mathbf{G}'$ [with indices $(l-1,m+1,n\pm1)$] in the ΓX-ΓX plane.

*Present address: Fritz Haber Institute der Max-Planck-Gesellschaft, Abteilung Oberflächenphysik, D-1000 Berlin 33, Germany.
†Telecom Research Laboratories, Clayton, Victoria, 3168 Australia.
‡Institut für Technische Physik, Universität Erlangen-Nürnberg, D-8520 Erlangen, Germany.

[1]G. V. Hansson and R. I. G. Uhrberg, Surf. Sci. Rep. **9**, 197 (1988).
[2]T.-C. Chiang, R. Ludeke, M. Aono, G. Landgren, F. J. Himpsel, and D. E. Eastman, Phys. Rev. B **27**, 4770 (1983).
[3]P. K. Larsen, J. F. van der Veen, A. Mazur, J. Pollmann, and B. H. Verbeek, Solid State Commun. **40**, 459 (1981).
[4]P. K. Larsen, J. F. van der Veen, A. Mazur, J. Pollmann, J. H. Neave, and B. A. Joyce, Phys. Rev. B **26**, 3222 (1982).
[5]P. K. Larsen, J. H. Neave, J. F. van der Veen, P. J. Dobson, and B. A. Joyce, Phys. Rev. B **27**, 4966 (1983).
[6]L. G. Salmon and T. N. Rhodin, J. Vac. Sci. Technol. B **1**, 736 (1983).
[7]J. Olde, G. Mante, H.-P. Barnscheidt, L. Kipp, J.-C. Kuhr, R. Manzke, M. Skibowski, J. Henk, and W. Schattke, Phys. Rev. B **41**, 9958 (1990).
[8]R. C. G. Leckey and J. D. Riley, CRC Crit. Rev. Solid State Sci. **17**, 307 (1992).
[9]For a discussion of momentum conservation in photoemission, see, for example, R. H. Williams, G. P. Srivastava, and I. T. McGovern, in *Electronic Properties of Surfaces*, edited by M. Prutton (Hilger, Bristol, 1984), p. 71.
[10]P. J. Feibelman and D. E. Eastman, Phys. Rev. B **10**, 4932 (1974).

[11]N. E. Christensen, Phys. Rev. B **30**, 5753 (1984); G. B. Bachelet and N. E. Christensen, *ibid.* **31**, 879 (1985).
[12]A. P. J. Stampfl, G. Kemister, R. C. G. Leckey, J. D. Riley, P. J. Orders, F. U. Hillebrecht, J. Fraxedas, and L. Ley, J. Vac. Sci. Technol. A **7**, 2525 (1989).
[13]W. Ranke and K. Jacobi, Prog. Surf. Sci. **10**, 1 (1981).
[14]R. C. G. Leckey, J. Electron Spectrosc. Relat. Phenom. **43**, 183 (1987).
[15]A. M. Bradshaw, W. Braun, W. Buchholz, R. Fröhling, A. Gaupp, W. Peatman, H. Petersen, J. Pflüger, F. Schäfers, and F.-P. Wolf (unpublished).
[16]G. P. Williams, F. Cerrina, G. J. Lapeyre, J. R. Anderson, R. J. Smith, and J. Hermanson, Phys. Rev. B **34**, 5548 (1986).
[17]R. D. Bringans and R. Z. Bachrach, in *Proceedings of the 17th International Conference on the Physics of Semiconductors,* edited by J. D. Chadi and W. A. Harrison (Springer-Verlag, New York, 1985), p. 67.
[18]H. Wern, R. Courths, G. Leschik, and S. Hüfner, Z. Phys. B **60**, 293 (1985).
[19]G. D. Mahan, Phys. Rev. B **2**, 4334 (1970).
[20]F. J. Himpsel, Appl. Opt. **19**, 3964 (1980).
[21]This is also a limitation of the three-step model. In fact, it cannot explain any phenomena in which the presence of the surface affects the wave functions of the initial or final states. Excitation from a bulk initial state into an evanescent final state,[10] for example, cannot be included in this model. One has to consider photoemission as a one-step process in order to include the effect of the surface periodicity in the interband transition.
[22]J. Pollmann and Sokrates T. Pantelides, Phys. Rev. B **18**, 5524 (1978).
[23]A. P. J. Stampfl, Ph.D. thesis, La Trobe University, (1991).
[24]H. U. Middlemann, L. Sorba, V. Hinkel, and K. Horn, Phys. Rev. B **35**, 718 (1987).
[25]J. Fraxedas, A. Stampfl, R. C. G. Leckey, J. D. Riley, and L. Ley, Phys. Rev. B **42**, 8966 (1990).
[26]C. M. Stampfl, Ph.D. thesis, La Trobe University (1991).
[27]X. D. Zhang, R. C. G. Leckey, and J. D. Riley (unpublished).

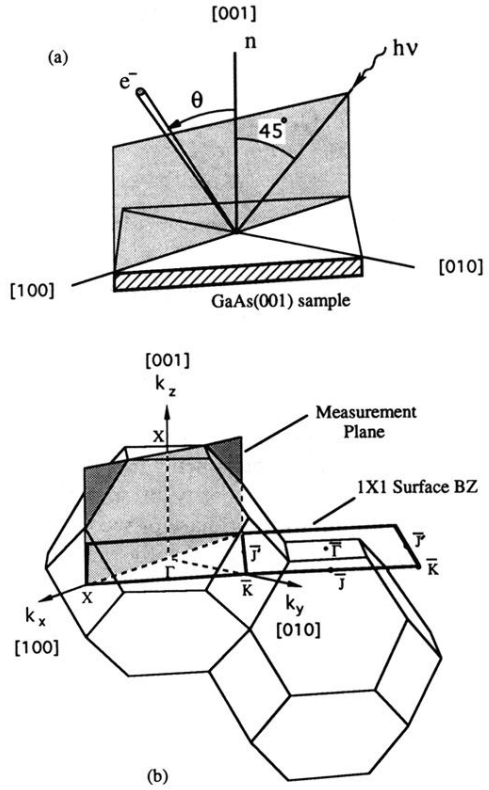

FIG. 1. (a) The experimental geometry and (b) the face-centered-cubic Brillouin zone in relation to the 1×1 surface Brillouin zone. The measurement plane is taken along the [100] azimuth.

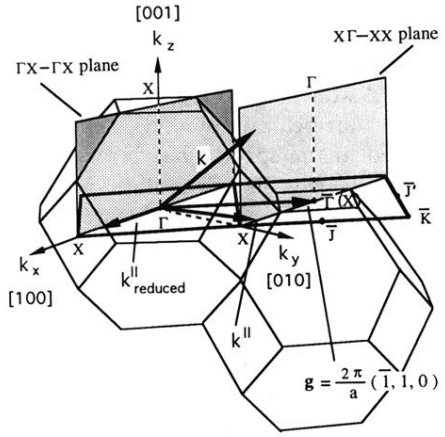

FIG. 7. Illustration of the surface umklapp process involving the surface reciprocal vector $\mathbf{g}=(2\pi/a)(\bar{1},1,0)$ in k space. With the surface umklapp, optical transitions are confined in the $X\Gamma$-XX plane, but the excited electrons can be detected in the ΓX-ΓX plane.